Article

Laser-Induced Ignition and Combustion of Single Micron-Sized Al-Li Alloy Particles in High Pressure Air/N$_2$

Dunhui Xu [1], Fang Wang [2], Shengji Li [3], Xuefeng Huang [1,*], Heping Li [1,*] and Yanhui Guo [4]

1 Institute of Energy, Department of Physics, Hangzhou Dianzi University, Hangzhou 310018, China
2 Science and Technology on Aerospace Chemical Power Laboratory, Hubei Institute of Aerospace Chemotechnology, Xiangyang 441003, China
3 College of Materials and Environmental Engineering, Hangzhou Dianzi University, Hangzhou 310018, China
4 Department of Materials Science, Fudan University, Shanghai 200433, China
* Correspondence: xuefenghuang@hdu.edu.cn (X.H.); peacelee@hdu.edu.cn (H.L.)

Abstract: To solve the problems associated with micron-sized aluminum (Al), including sintering, agglomeration, and slag deposition during the combustion of aluminized propellants, aluminum–lithium (Al-Li) alloy, prepared by introducing a small amount of Li (1.0 wt.%) into Al, was used in place of Al. Then, the ignition and combustion characteristics of single micron-sized Al-Li alloy particles were investigated in detail using a self-built experimental apparatus and multiple characterization methods. The ignition probability, ignition delay time, flame propagation rate, burn time, combustion temperature, flame radiation spectra, and microexplosion characteristics were obtained. The TG-DSC results demonstrated that, as compared to the counterpart Al, the Al-Li alloy had a lower ignition temperature. The emission lines of AlO revealed the gas-phase combustion of the Al-Li alloy, and thus the Al-Li alloy exhibited a mixed combustion mode, including surface combustion and gas-phase combustion. Moreover, during combustion, a microexplosion occurred, which increased the combustion rate and reduced the burn lifetime. The ambient pressure had a significant effect on the ignition and combustion characteristics of the Al-Li alloy, and the ignition delay time and burn time exponentially decreased as the ambient pressure enhanced. The combustion temperature of the Al-Li alloy at atmospheric pressure was slightly higher than those at elevated pressures. The Al-Li alloy burned in N$_2$, but no microexplosion was observed. Finally, the ignition and combustion mechanism of the Al-Li alloy in air was demonstrated by combining SEM, EDS, and XRD analyses of the material and residues. The results suggest that the addition of Li promoted the combustion performance of Al by changing the surface structure of the oxide film and the combustion mode.

Keywords: metal fuels; Al-Li alloy; laser ignition; microexplosion; pressure effect

1. Introduction

Metal fuels, which are considered as fuel additives, have been widely applied in solid rocket propellants, explosives, and pyrotechnics [1,2]. Among them, Al has the advantages of good flammability, low oxygen consumption, and a high combustion temperature [3]. The micron-sized Al particles added into solid propellants can significantly improve the specific impulse [4–6]. However, with Al microparticles, sintering, agglomeration, and slag deposition phenomena occur on the propellant burning surface during combustion causing the agglomeration of aluminum and the formation of condensed combustion products (CCP) [7–9]. The agglomeration size is several orders of magnitude larger than the original Al microparticles, possibly resulting in two-phase flow loss and the ablation of the insulation layer and nozzle in solid rocket motors.

Many new strategies have been proposed to solve these problems. Nanometer Al powder was used to replace micron-sized Al in propellants; however, agglomeration and

sintering still occurred, and a low active Al content and incomplete combustion reduced the comprehensive performance of the propellants [10–12]. By adding other substances, such as a nanopolymer, into Al powder, the microexplosion of Al can be induced on the propellant surface, reducing sintering and agglomeration [9,13,14]. However, the incorporated polymer chemically reacts with Al, which can cause safety concerns when in storage. Another feasible strategy is to activate the surface of micron-sized Al or adopt surface coating to increase the active Al content. For example, coating a layer of nickel on the surface of Al microparticles to replace the alumina layer can increase the active Al content by ~4% [15]. An Fe-Al composite powder with an electroless coating was prepared to improve the energy release rate of fuel [16]. The iron coating of the Al-based alloy powder was used to improve its thermal properties and aging stability [17]. A low-density polyethylene coating was synthesized to modify and activate Al, shorten the residence time of particles on the propellant surface, induce the microexplosion, and reduce agglomeration [18].

In recent years, micron-sized Al-based binary alloys have received much attention. Alloying treatments can not only significantly improve combustion efficiency, but also control the ignition and combustion characteristics by adjusting the content of each component, such as in Al-Ti, Al-Zr, Al-Mg, and Al-Li alloys [19–25]. Shoshin et al. [20,21] prepared Al-Ti composites and tested their ignition temperature and combustion rate. The results showed that the ignition temperature of Al-Ti composites was significantly lower, and the combustion rate was higher compared to Al. Huang et al. [23] demonstrated that, when Mg was added to Al to form the alloy, the combustion of Mg came before that of Al, an obvious microexplosion phenomenon was observed, and, thus, combustion efficiency was significantly improved. Metal Li has a larger difference in melting and boiling points and higher reactivity compared with Al, which can react with many gaseous substances, including nitrogen (N_2), and is considered as one of the most promising formulations for energetic material applications. Moreover, lithium oxide is porous, and it provides more channels for oxidizing gas to diffuse inward, which is conducive to more of the active Al content participating in the reaction [24–26]. Blackman et al. [27] observed the vigorous microexplosion behavior of Al-Li alloy microparticles (10 wt.% Li). A recent study showed that Al-Li alloy (20 wt.% Li), when used as a fuel additive for ammonium perchlorate composite propellant (APCP), improved the combustion performance and demonstrated environmentally friendly benefits [17]. Terry et al. [28,29] studied the combustion phenomenon of adding Al-Li alloy fuel into the propellant, and further showed that the addition of Al-Li alloy could reduce the loss of two-phase flow and improve the combustion efficiency.

Although the literature demonstrates the excellent properties and application prospects of Al-Li alloy, the factors affecting the ignition and combustion of Al-Li binary alloy have not been fully studied, such as the pressure effect and particle effect. Moreover, the ignition and combustion mechanisms are not deeply understood, especially for individual isolated microparticles. Therefore, this paper focuses on the ignition and combustion characteristics of single micron-sized Al-Li alloy particles. Firstly, the characterization of as-prepared Al-Li alloy microparticles was performed using optical microscopy, a scanning electron microscope (SEM), an energy dispersive spectrometer (EDS), X-ray diffraction (XRD), and the thermogravimetric and differential thermogravimetric (TG-DTG) and differential scanning calorimeter (DSC) techniques to obtain the size distribution, morphology, composition, crystal structure, ignition temperature, activation energy, and thermal stability. Secondly, an experimental setup including precise laser ignition, microscopic high-speed cinematography, three-color pyrometer, and flame emission spectrum detection modules was built to obtain the ignition probability, ignition delay time, flame propagation rate, combustion time, combustion temperature, and flame radiation spectra, and analyze the evolution of combustion and microexplosion phenomena in individual Al-Li alloy microparticles. Moreover, the pressure effect (0.1~0.8 MPa) on the ignition and combustion properties of Al-Li alloy in air was studied. Ignition and combustion experiments in N_2 were also con-

ducted to reveal the reaction behavior of Al-Li and N_2. The morphology and composition of residues were characterized by SEM and EDS. Finally, a general combustion route was proposed to explain the mechanism of ignition and combustion of individual micron-sized Al-Li alloy particles.

2. Materials and Methods

2.1. Material Characterization

Micron-sized Al-Li alloy particles with a mass ratio of 99% Al and 1% Li were prepared using the melt atomization method [23]. The quantitative aluminum and lithium blocks were crushed and then heated in the high frequency induction furnace with argon gas. The molten Al-Li alloy flowed along the duct and arrived at the nozzle. The atomized alloy droplets were cooled with argon gas and solidified to form powder particles with high sphericity. The SEM (Sigma 300, ZEISS, Oberkochen, Germany) characterization (Figure 1) demonstrates that Al-Li alloy microparticles had high sphericity and a grid-like surface pattern. This means that there was significant diffusion or intermetallic formation between the constituents to guarantee the homogeneity of physicochemical properties. The EDS (Sigma 300, ZEISS, Oberkochen, Germany) test (Figure 2) shows that the Al content of the Al-Li alloy powder was approximately 99%, but the Li content could not be accurately measured. The existence of the oxygen element in the alloy particles means that there was slight oxidation on the surface.
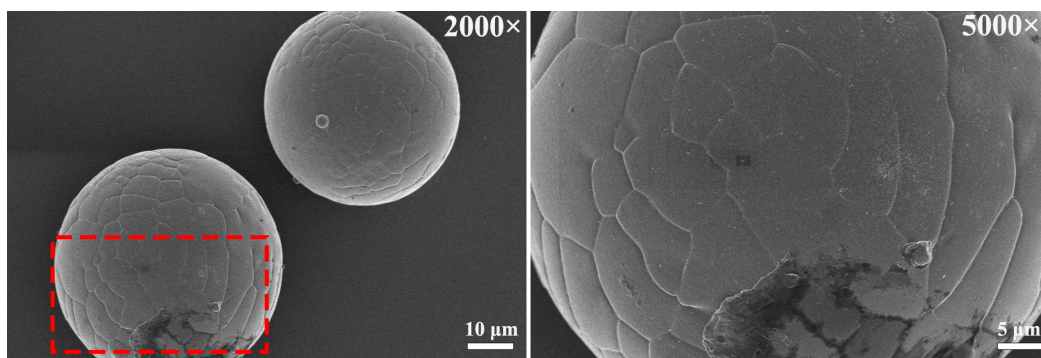

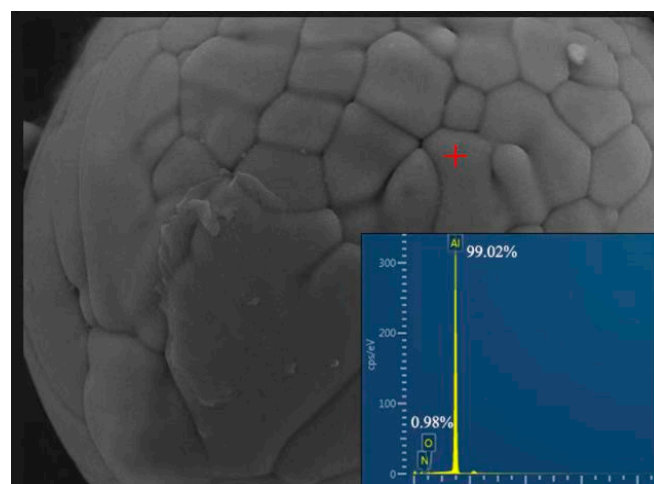**Figure 1.** SEM morphology of Al-Li alloy microparticles.

**Figure 2.** EDS analysis of Al-Li alloy microparticles.

The X-ray diffraction (XRD, Phaser, Bruker D2, Karlsruhe, Germany) pattern (Figure 3) of the Al-Li alloy powder shows that there were five characteristic diffraction peaks at 38.66°, 44.90°, 65.24°, 78.37°, and 82.58°. The peaks marked as "1" were attributed to

Al [30]. The weak characteristic diffraction peaks at 34.81° in the magnified subplot marked as "2" was attributed to Li_2O_2.
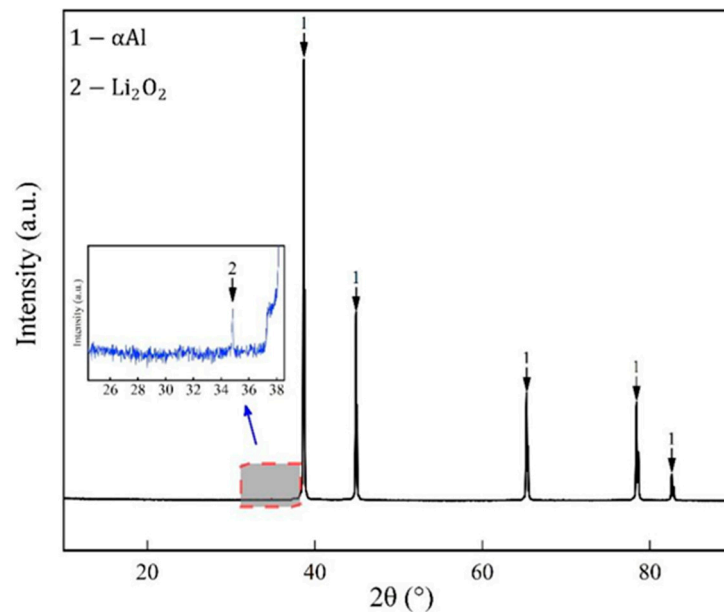
Figure 3. The XRD pattern of Al-Li alloy microparticles.

In this work, 80 isolated micron-sized Al-Li alloy particles were randomly selected, and their sizes were tested using a calibrated optical microscope. Figure 4 shows that the size distribution of these Al-Li alloy microparticles ranged from 30 μm to 80 μm, and the average particle size was 54.3 μm. In order to weaken the effect of particle size on the ignition and combustion characteristics, only 45~55 μm Al-Li alloy particles were selected for the tests.
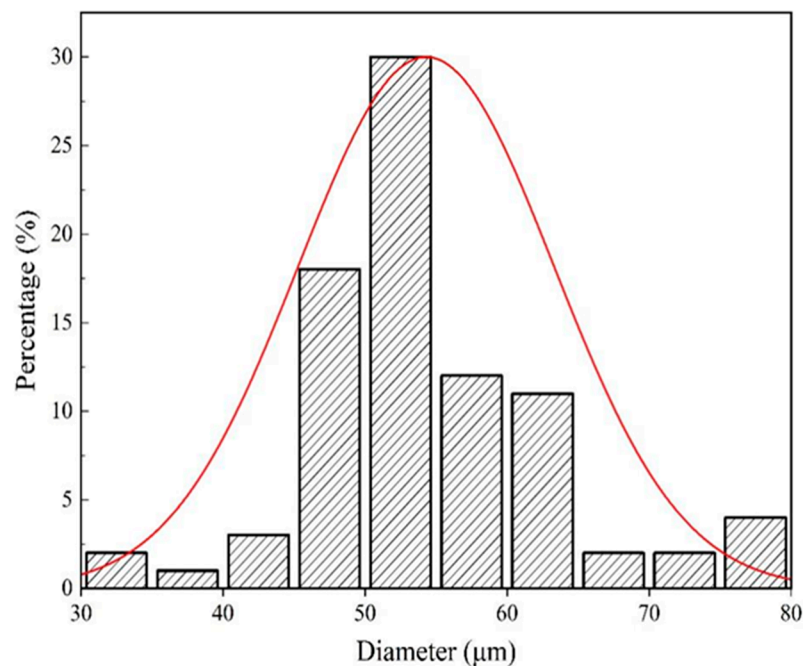
Figure 4. The size distribution of Al-Li alloy microparticles.

2.2. Experimental Setup for Ignition and Combustion Characterization

Figure 5 shows the schematic of the experimental setup for characterizing the ignition and combustion of single Al-Li alloy microparticles, including precise laser ignition, microscopic high-speed cinematography, three-color pyrometer, and flame emission spectrum detection modules. The laser, high-speed camera, pyrometer, and spectrometer could be accurately triggered using a digital delay generator.
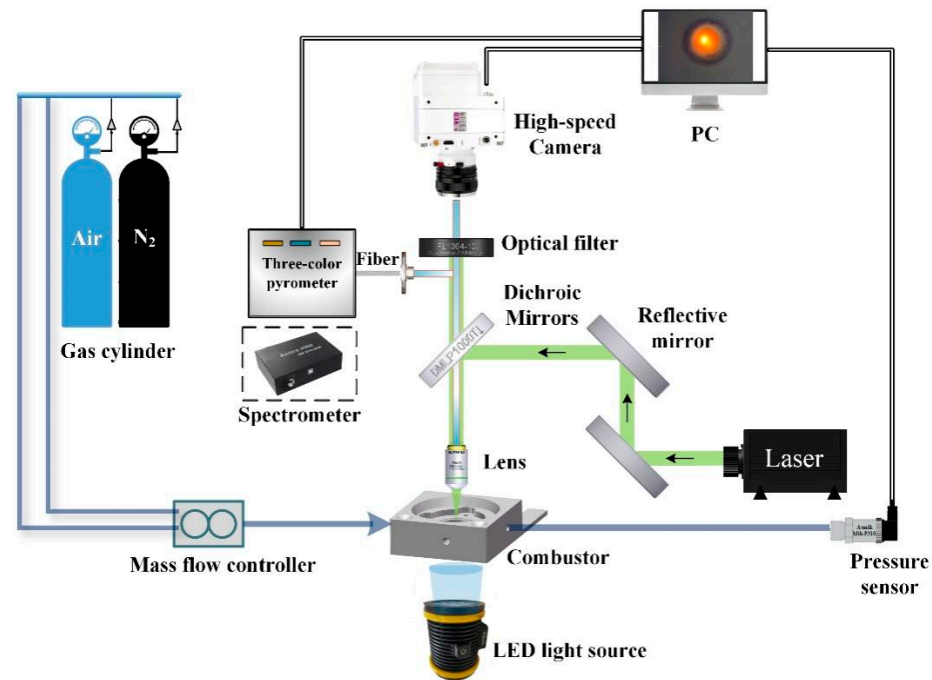

Figure 5. Schematic of experimental setup.

For the precise laser ignition module, the laser beam emitted from the laser had a wavelength of 1064 nm and was in TEM_{00} mode (New Industries Optoelectronics Tech. Co. Ltd., Changchun, China). It was elevated by two total reflection mirrors, passed through a dichroic and an objective (20×), and perpendicularly entered the combustion chamber to ignite the Al-Li alloy microparticles. The focused laser beam's diameter was ~18.8 μm. The ignition power (density) could be precisely adjusted by varying the modulated laser output power from 0 to 2000 mW, ranging from 0 to 7.21×10^5 W/cm^2.

Microscopic high-speed cinematography module includes a 20× objective (Olympus, Tokyo, Japan), dichroic, notch filter, high-speed camera (Phantom VEO E310L, Vision Research Inc., Wayne, NJ, USA), and LED light source. The numerical aperture (NA) of the objective was 0.40, and the spatial solution was ~0.69 μm. A high-speed camera was used to capture the images and videos of burning Al-Li alloy microparticles. For clear imaging, a LED light source (Constellation 120E, Integrated Design Tools Inc., Pasadena, CA, USA) was used to illuminate the combustor and the microparticles. A notch filter was installed in front of the high-speed camera, which was able to effectively weaken the influence of the laser on microparticle and flame imaging. To observe the variations of microparticle and flame morphology during combustion, the high-speed camera was set at a shooting frame rate of 10,000 fps and an exposure time of 40 μs.

A three-color pyrometer module was installed to measure the flame temperature during combustion. Since the flame radiation of an individual burned microparticle is relatively weak, three photomultiplier tubes (PMTs) in the pyrometer were selected to assess the flame signals. To avoid the characteristic radiation bands of the metals and combustion products, the wavelengths of 430 nm, 660 nm, and 750 nm were chosen. An armor optical fiber was connected to the pyrometer to receive the flame radiation signal

and weaken the background light. The temporal resolution of the three-color pyrometer was maintained at 50 µs.

A flame emission spectrum detection module was used to detect the emission spectra of the combustion products, which contained a receiving fiber, splitter, and grating spectrometer. The fiber received the flame signals and transferred them into the grating spectrometer through the splitter. The spectral resolution of the grating spectrometer was 0.75 nm.

The combustion chamber was made of aluminum alloy. The observation windows were set on the top and bottom surfaces of the combustion chamber. On the left side, the combustor was connected with the intake pipe. The different gases could be delivered to the combustion chamber through the pressure relief valve and mass flow controller. The combustor worked at a maximum pressure of 1.0 MPa. The pressure in the combustion chamber was monitored in real time online using a digit pressure sensor.

During experiments, many Al-Li alloy microparticles were put into the combustor and dispersed on the bottom surface using a home-made tool to ensure that an individual microparticle was isolated. The isolated microparticle was moved to the focal point of the objective using a sample stage with 3-axis (X, Y, and Z) translation. The laser and the detectors were triggered by the digital delay generator to ignite the microparticle and simultaneously acquire the flame signals.

3. Results and Discussion

3.1. Ignition Characteristics

3.1.1. Thermal Analysis and Ignition Temperature

The TG-DSC (STA 6000, PerkinElmer, Waltham, MA, USA) thermal analysis experiments of the Al-Li alloy were conducted from 30 °C to 1200 °C in air with a heating rate of 10 °C /min. As a comparison, the thermal analysis of Al with a similar particle size distribution and an average particle size of 57.4 µm was carried out in the same operation conditions. The TG data (Figure 6a) demonstrate that the oxidation reaction process of Al-Li alloy in air could be roughly divided into three stages, i.e., the early stage of the reaction, the slow reaction period, and the violent reaction period. In the 1st stage, the weight gain of the sample remained basically unchanged from 30 °C to ~400 °C. In the 2nd stage there was a weight gain of 3.5%, and the weight gain rate reached the maximum value of 0.43%/min at 695 °C. In the 3rd stage, the weight gain reached 75.1% at a maximum rate of 5.53%/min at 1029 °C. Compared with the Al-Li alloy, the oxidation of Al went through similar stages. The first stage was the same, while the transition temperature and weight gain in the 2nd and 3rd stages significantly differed from those of Al-Li. The maximum weight gain rates of Al were 0.05%/min at 584 °C in the 2nd stage and 0.21%/min at 1047 °C in the 3rd stage. The total weight gain was only 3.2%. The DSC data (Figure 6a) illustrate that the Al-Li alloy had one obvious endothermic reaction at the peak temperature of 660 °C and two significant exothermic reactions at the peak temperatures of 698 °C and 1026 °C, respectively. The Al had the same endothermic peak temperature as the Al-Li alloy (660 °C), while no obvious exothermic peak was observed. The comparison of the thermal analysis shows that the initial oxidation of the Al-Li alloy was slower than that of Al, while the later oxidation was much stronger and the released energy was higher, suggesting that the addition of Li promotes more Al content to participate in the oxidation reaction in air at high temperatures.
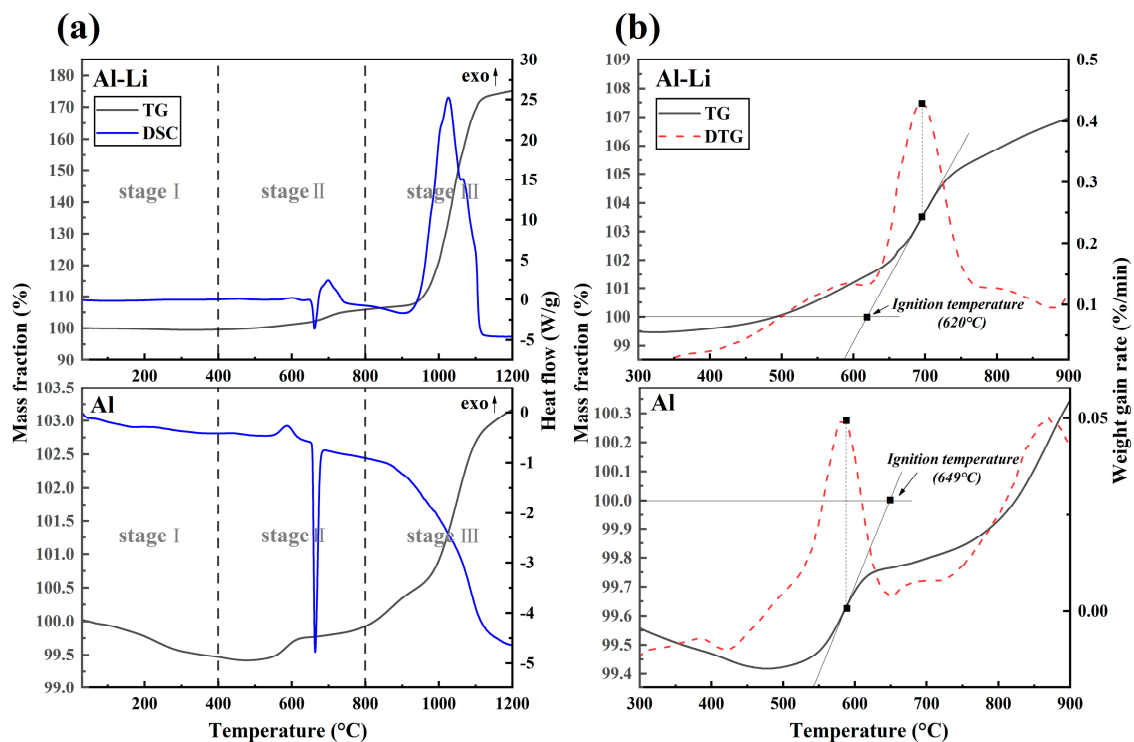
Figure 6. Thermal analysis curves of Al-Li alloy and Al powder in air: (**a**) TG-DSC; (**b**) TG-DTG.

The ignition temperature of Al-Li alloy microparticles can be calculated using the tangent method [31–33]. In order to eliminate the process of small weight loss due to surface hydrolytic adsorption and the dehydroxylation of amorphous alumina before sample weight gain, the initial mass (100%) was chosen as the reference line. The ignition temperature of the Al-Li alloy (~620 °C) was lower than that of Al (~649 °C), and both of them were below the melting point of Al (660 °C) (Figure 6b), which means that a rapid oxidation reaction occurred earlier than melting. It might be inferred that the alloy phase separation occurred before the ignition.

3.1.2. Ignition Power (Density) Threshold

The ignition power (density) affects the ignition probability of individual micron-sized Al-Li alloy particles. When the ignition power (density) is not high enough, ignition cannot occur. For the laser-induced ignition of individual micron-sized particles in cool air, as the highly focused laser beam acts on an individual microparticle, the microparticle receives from the photophoretic force generated by the laser irradiation [34] and can be pushed away from the focal point, resulting in ignition failure. In this work, at different laser powers (1600 mW, 1300 mW, 800 mW, 700 mW, 600 mW) with a beam diameter of ~18.8 μm, laser-induced ignition experiments for Al-Li alloy microparticles with diameters of 45–55 μm in air were conducted. At each laser power (density), 20 individual Al-Li alloy microparticles were selected to carry out the experiments. If a visible spark followed by a continuous flame were observed, it was recorded as a successful ignition, otherwise, it was recorded as a failed ignition. The statistical ignition probability is listed in Table 1. Al-Li alloy microparticles failed to ignite when the laser power (density) was 600 mW (2.16×10^5 W/cm^2). While at 700 mW (2.52×10^5 W/cm^2), some particles ignited. It was demonstrated that the lowest laser ignition power (ignition power threshold) of Al-Li alloy microparticles of 45–55 μm was between 600 mW and 700 mW ($2.16~2.52 \times 10^5$ W/cm^2). The ignition probability of Al-Li alloy microparticles increased with increasing laser ignition power. When the laser power (density) was maintained at 1600 mW (5.77×10^5 W/cm^2), the ignition probability of Al-Li alloy microparticles reached 95%, but not 100%. The reason may be that the photophoretic force pushed the microparticles away from the focused

beam, which led to ignition failure. To further ensure that the Al-Li alloy microparticle was ignited, the ignition power was maintained at the maximum power of 2000 mW (7.21×10^5 W/cm^2) in the following experiments.

Table 1. Ignition probability of single Al-Li alloy microparticles at different ignition powers.

Ignition Power (mW)	Ignition Power Density ($\times 10^5$ W/cm^2)	Experimental Runs (Round)	Ignition Runs (Round)	Ignition Probability
1600	5.77	20	19	95%
1300	4.69	20	15	75%
800	2.88	20	12	60%
700	2.52	20	9	45%
600	2.16	20	0	0

3.1.3. Ignition Delay Time

Since the laser, three-color pyrometer, and high-speed camera were triggered synchronously, the ignition delay time (t_i) of an individual microparticle could be measured using two methods. One method is based on the analysis of the image taken by the high-speed camera. When the laser acts on the microparticles, it is the moment of ignition initiation. When an obvious visible flame is observed on the microparticle surface, it is determined as the ignition moment. The time difference between the two moments is called the ignition delay time. The other one depends on the analysis of the radiation signal from the PMT in the three-color pyrometer [35]. The moment that the PMT collects the radiation signal is the ignition moment, thus the time difference between the two moments, i.e., the PMT signal and laser onset, is the ignition delay time. The ignition delay time based on the two methods was in good agreement through the experimental tests, and the relative error was below 5%.

The ignition delay time depends on many factors, including the properties of fuel, ignition parameter, and operation conditions. In this work, via repetitive tests and the analysis of the image taken by the high-speed camera (the first measurement method), the ignition delay time of the Al-Li alloy (45–55 μm) in air at atmospheric pressure and room temperature ranged from ~0.2 s to ~2.0 s at the ignition power of 700~2000 mW (power density of 2.52~7.21×10^5 W/cm^2), with no clear correlation between ignition delay time and laser power.

3.1.4. Pressure Effect on Ignition Delay Time

Ambient pressure plays a key role in influencing the ignition performance of propellants. Therefore, in the experiment, the pressure effect on the ignition of single Al-Li alloy microparticles was assessed. The operating pressure of the combustion chamber was maintained at 0.1 MPa, 0.4 MPa, 0.6 MPa, and 0.8 MPa. The laser was then turned on to ignite the Al-Li alloy microparticles. To ensure that each Al-Li alloy microparticle ignited, the laser power was enhanced to 2000 mW (power density of 7.21×10^5 W/cm^2).

Similarly, at each pressure, 20 Al-Li alloy microparticles were chosen to conduct the ignition experiments. Figure 7 shows the average ignition delay time of the Al-Li alloy microparticles at different air pressures. The error mainly resulted from the difference in the microparticle size, i.e., 45–55 μm. Compared with the ignition characteristics at 0.1 MPa, when the combustion chamber pressure was elevated to 0.4 MPa, 0.6 MPa, and 0.8 MPa, the average ignition delay time was reduced by 34.0%, 51.0% and 57.4%, respectively. The relationship between the average ignition delay time (t_{ai}) and the air pressure (p) can be fitted as follows:

$$t_{ai} = 0.07732 + 0.47069e^{-1.69422p} \left(R^2 = 0.996 \right) \tag{1}$$
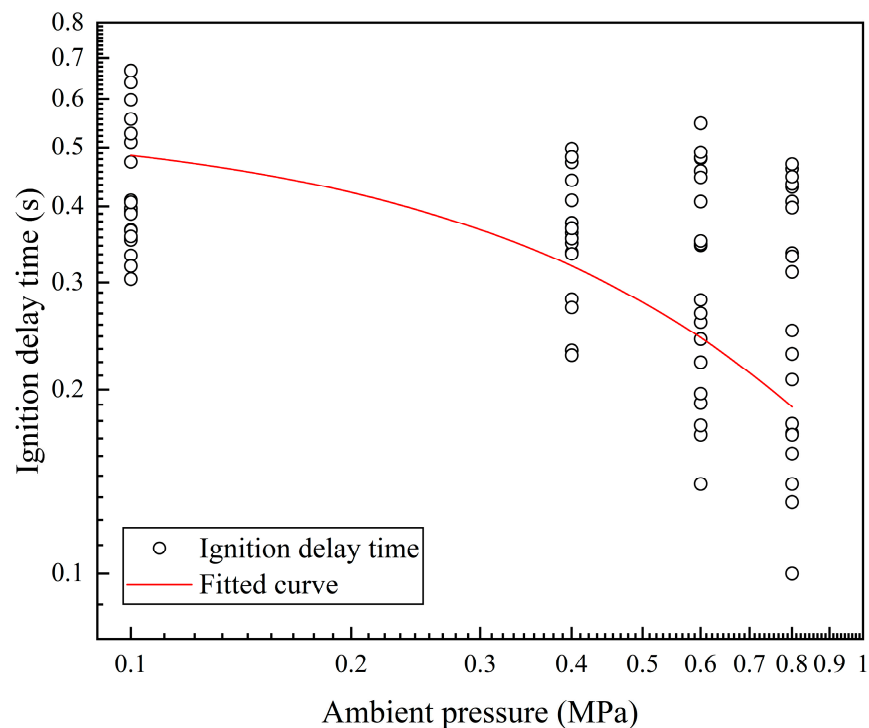
**Figure 7.** The ignition delay time of single Al-Li alloy microparticles at different ambient pressures.

The function shows that the ignition delay time of Al-Li alloy microparticles decays exponentially as the air pressure increases.

Ignition data for pure Al could not be obtained in the current study because of the difficulty in finding individual pure aluminum particles with a high circularity. Comparisons with previous correlations are not included here because of the difference in experimental setups.

3.2. Combustion Characteristics

3.2.1. Combustion Evolution

Figure 8 shows the representative snapshots of the combustion process of a single Al-Li alloy microparticle with a particle size of ~55 μm in air. The video can be found in Supplementary Material Video S1. It was found that the combustion evolution of the Al-Li alloy microparticle can be divided into the melting and expansion (Figure 8a–c), gasification (Figure 8d,e), diffusion combustion (Figure 8f,g), and extinction (Figure 8h) stages. During diffusion combustion, the microexplosion was clearly observed (white arrows in Figure 8f,g), and there were molten daughter droplets that were quickly ejected from the mother droplet that dispersed on the base. Terry et al. [29] confirmed the microexplosion behavior of Al-Li alloy droplets and found that the molten aggregated droplets in the propellants can be ejected from the surface layer through dispersion boiling. The occurrence of a microexplosion is due to the significant differences between the melting and boiling points of Li and Al. Moreover, owing to the high reactivity of Li, Li reacts with the oxidant to form loose and porous oxide layers (Li_2O, $LiAlO_2$, Li_2CO_3) [36,37], which form cavities on the dense oxide layer (Al_2O_3) earlier, and thus shorten the ignition delay time of the microparticles and increase the probability of a microexplosion.
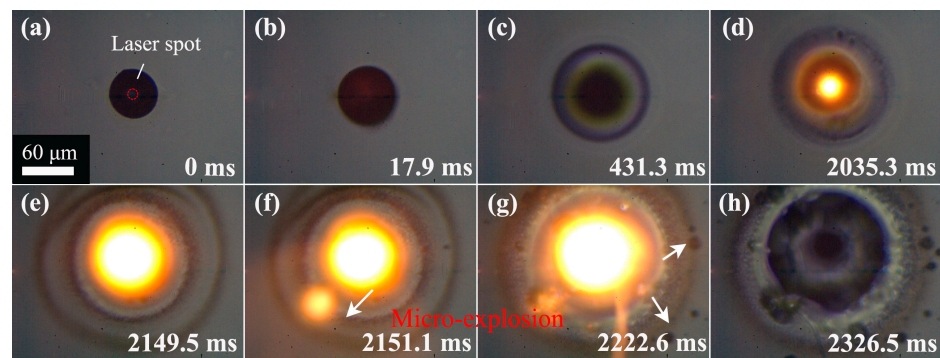
Figure 8. (**a**–**h**) Representative snapshots during the combustion of a single Al-Li alloy.
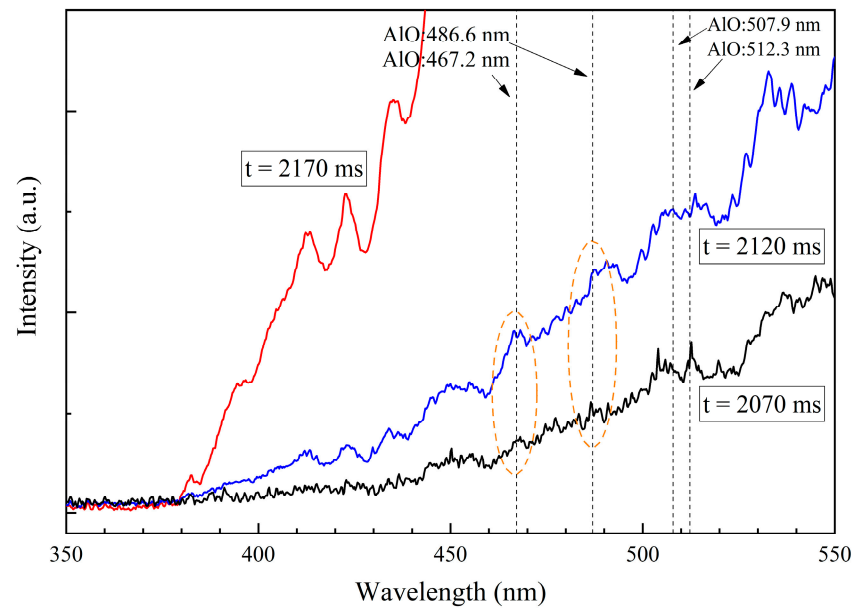
3.2.2. Flame Characteristics

Using the R-value of the image pixels, the image was binarized and the edges of the flame and the flame area were identified [38]. The flame areas (Figure 9) demonstrated that the single Al-Li alloy microparticle in air burned locally (1874–2000 ms), and the smallest flame area appeared at the ignition moment, i.e., ~0.0056 mm^2. However, after ignition, the flame rapidly propagated and the flame area obviously enlarged in 2014 ms. The combustion flame tended to be stable at 2154 ms, and the flame structures observed from a vertical view were approximately circular. The maximum flame area was maintained at ~1.0 mm^2. After 2334 ms, with the consumption of the fuel, the heat dissipation loss gradually exceeded the generated heat, and thus the flame area gradually decreased until it extinguished. This suggests that the combustion behavior of Al-Li alloy microparticles in a stagnant air flow is mainly characterized as a mixed mode, including heterogeneous surface combustion and homogeneous gas-phase combustion, which is different from the heterogeneous surface combustion mode of Al [30].
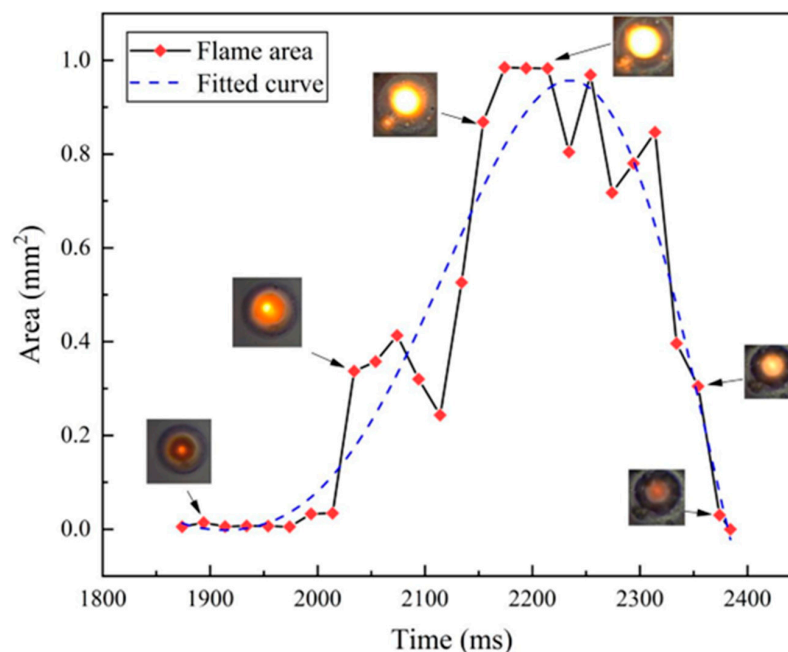
Figure 9. Flame propagation and areas denoting of a single burned Al-Li alloy microparticle.

The representative time-resolved flame radiation spectrum of a single Al-Li alloy microparticle acquired with the grating spectrometer is shown in Figure 10. According to the NIST atomic spectrometric database and references [39], these emission lines at 467.2 nm, 486.6 nm, 507.9 nm, and 512.3 nm can be attributed to AlO, which is the main gas-phase

intermediate product of Al combustion. The radiation intensity gradually increased as the combustion evolved. This shows that the Al-Li alloy underwent gas-phase combustion [39].

Figure 10. Representative time-resolved spectra and characteristic emission lines of AlO.

3.2.3. Pressure Effect on the Combustion

Figure 11 shows the representative snapshots of the combustion flame of single Al-Li alloy microparticles in pressurized air atmospheres of 0.4 MPa, 0.6 MPa, and 0.8 MPa. In the atmosphere of 0.4 MPa, after the laser was turned on, the microparticle was heated and began to melt. At 87.4 ms, a bright yellow gas-phase flame was observed above the microparticle (Figure 11(c1)). The gas-phase flame rapidly propagated and covered the whole particle (Figure 11(f1)). Simultaneously, the molten liquid droplets were ejected and sprayed in tiny droplets, and an obvious microexplosion was observed (Figure 11(f1–h1)). The final combustion products (Figure 11(i1)) appeared circular, suggesting that the gas-phase products homogeneously diffused and condensed in cool air, and a vigorous microexplosion occurred. In the atmospheres of 0.6 MPa and 0.8 MPa, the flame demonstrated similar propagation characteristics. While the maximum flame area became smaller, the time to reach the maximum flame area was shortened, and the distributed zone of the final combustion products gradually shrank.
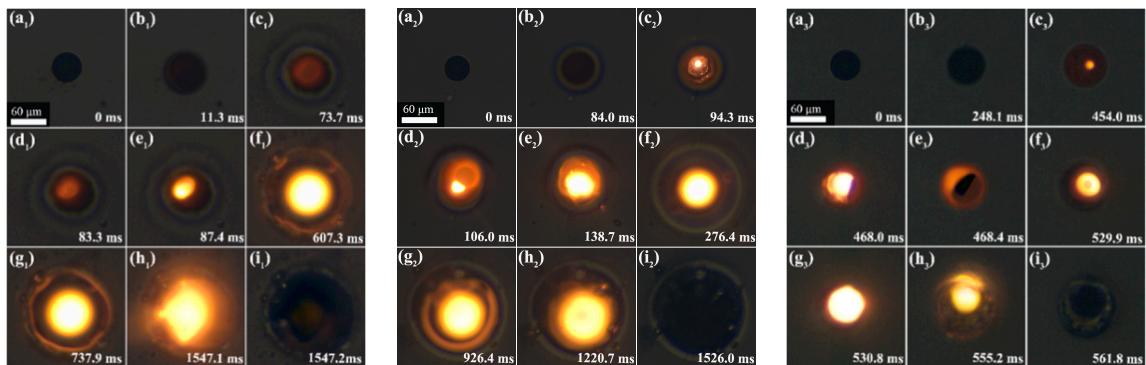
Figure 11. Representative snapshots of flame sequences during the whole combustion process of single Al-Li alloy microparticles at 0.4 MPa (left (**a₁**–**i₁**)), 0.6 MPa (middle (**a₂**–**i₂**)), and 0.8 MPa (right (**a₃**–**i₃**)).

The increase in the ambient pressure can slightly increase the combustion rate of pure Al particles, thus achieving a shorter combustion time [40,41]. The burn time (t_b) of an individual Al-Li alloy microparticle with varying ambient pressures is shown in Figure 12. The burn time can be measured using two methods, similar to the definition of the ignition delay time in Section 3.1. Compared with the burn time at 0.1 MPa, the burn time at an elevated air pressure was lower. The ambient pressure not only affects the reaction rate, but also the diffusion rate. Kuryavtsev et al. [42] proposed a three-zone model of Al combustion to explain how the oxidant diffuses into the microparticles and demonstrated that the pressure would affect the binary diffusion rate in the outer region of the condensed particles. According to classical diffusion theory, at low pressure (0.1 MPa), the average free path of gas molecules is much larger than that at higher pressure; thus, the diffusion coefficient is lower. When the pressure increases, the addition of highly reactive Li further promotes the diffusion of oxidants into the particles, resulting in a shorter burn time.
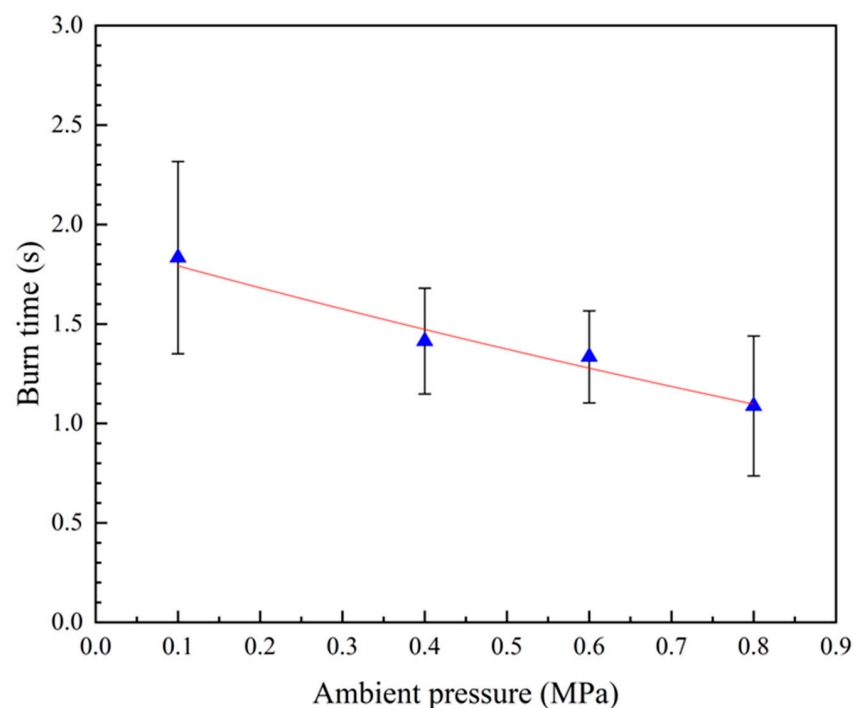
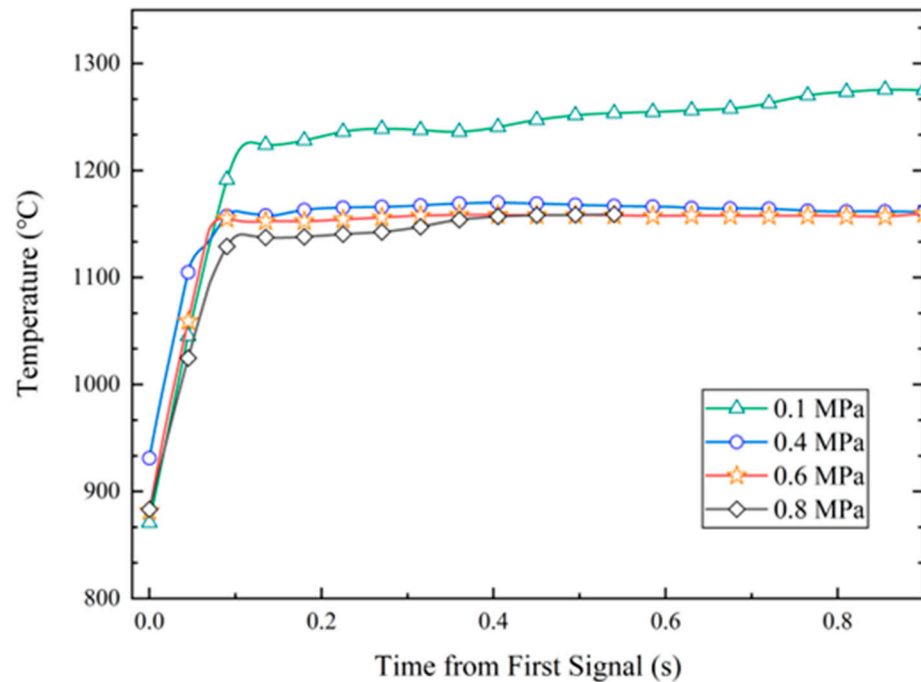**Figure 12.** The burn time of single Al-Li alloy microparticles at different ambient pressures.

The relationship between the burn time $t_b(ms)$ and the pressure p (atm) could be fitted and expressed as:

$$t_b = \frac{1874.59}{p^{0.1799}} \qquad (2)$$

In this work, thus, the burn time is a power function of the pressure, i.e., $t_b \propto \frac{1}{p^{0.1799}}$, which is in good agreement with the results in the literature (M.W. Beckstead [40] $t_b \propto \frac{1}{p^{0.1}}$, Alexandre Braconnier [41] $t_b \propto \frac{1}{p^{0.12}}$).

The temporal histories of the flame temperature of single Al-Li alloy microparticles during combustion (Figure 13) demonstrated that the combustion included a rise period and a stable period. In the rise stage, the temperature rise rates at high pressure were approximate to those at low pressure, at an order of magnitude of 10^3 K/s. In the stable stage, the combustion temperature at 0.4 MPa, 0.6 MPa, and 0.8 MPa were obviously lower than that at 0.1 MPa. At high pressure, the maximum combustion temperatures were almost equivalent: 1170.0 °C (0.4 MPa), 1163.3 °C (0.6 MPa), and 1167.4 °C (0.8 MPa), respectively. The maximum combustion temperature at 0.1 MPa reached 1282.8 °C. In pressurized air at room temperature, because Al-Li alloy microparticles were more prone

to microexplosion, unburned molten droplets were constantly ejected from the interior of the microparticles during combustion, and the microparticle oxidation reaction degree was weakened, resulting in a lower heat release rate. This suggests that the elevated air pressure balanced the microexplosion intensity, the combustion temperature, and the burn time of the Al-Li alloy microparticles in cool air.

Figure 13. Representative temperature of single Al-Li alloy at different ambient pressures (signal has been smoothed).

3.2.4. Combustion Residues

The SEM morphology of an incompletely burned-out Al-Li alloy microparticle is shown in Figure 14. Cracking of the oxide layer and a certain degree of sintering with the substrate can be clearly observed. It can be inferred that, as the reaction proceeded, the oxidizing gases in the air continued to diffuse inward through the cracks and react with the active Al and Li in the shell. Further EDS mapping analysis (Figure 15) of the Al-Li alloy residue shows a relatively uniform distribution of elements. The daughter particles ejected from the mother particle due to the microexplosion were also characterized by SEM and EDS. The SEM photograph (Figure 16a) shows that several particles with a large size were located at the center and tiny particles were located at the periphery. Among these residues, the tiny particles with white burrs may be condensed Al and Al_2O_3 (Figure 16b). The EDS analysis (Figure 17) shows that the mass ratios of Al, O, and N in the combustion residues were 34.84%, 64.97%, and 0.19%, respectively. The mass ratio of oxygen atoms is higher than the oxygen content (47.06%) in Al_2O_3, indicating that the oxygen not only reacted with Al, but also with Li or other elements contained in the glass substrate of the combustion chamber, such as C, Si, Ca, etc. (Figure 17b).
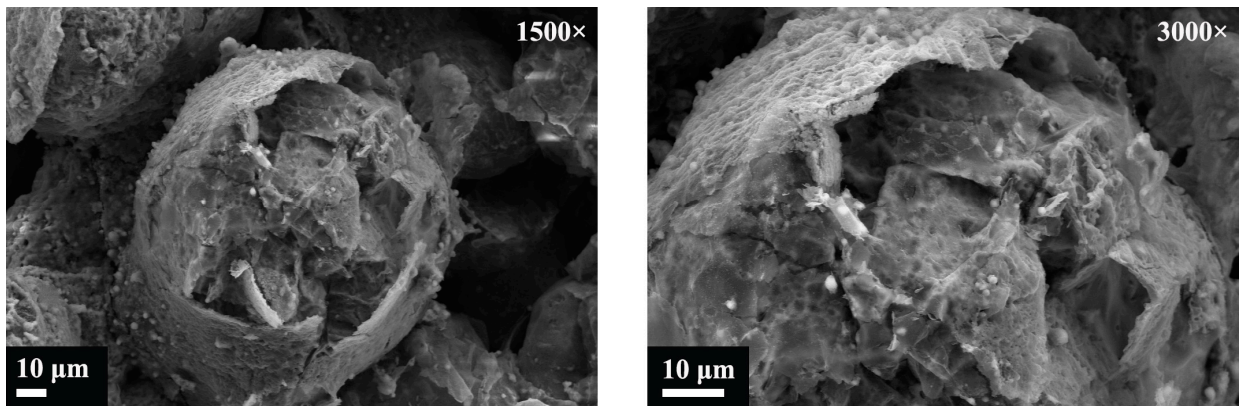
Figure 14. SEM photographs of combustion residues of a single Al-Li alloy microparticle.
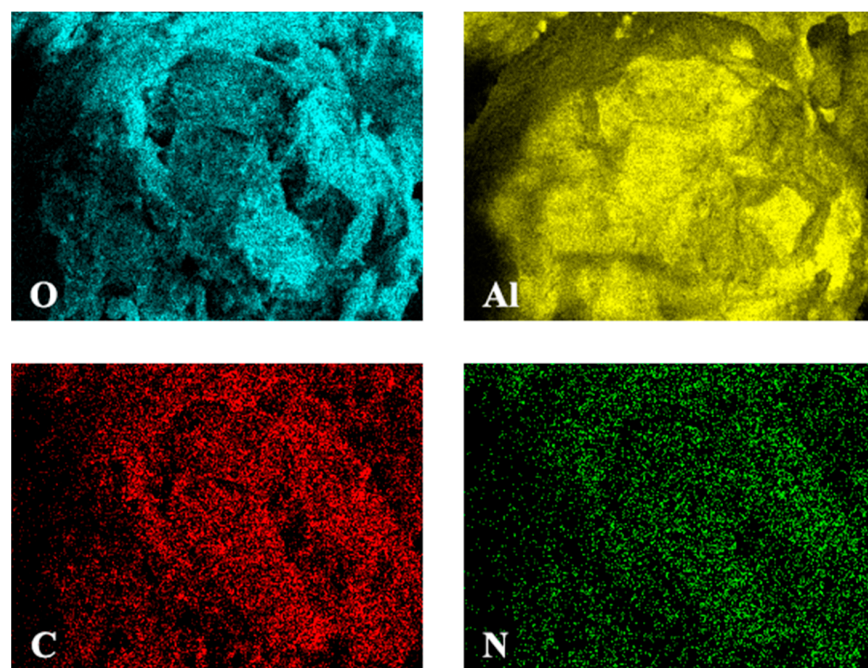

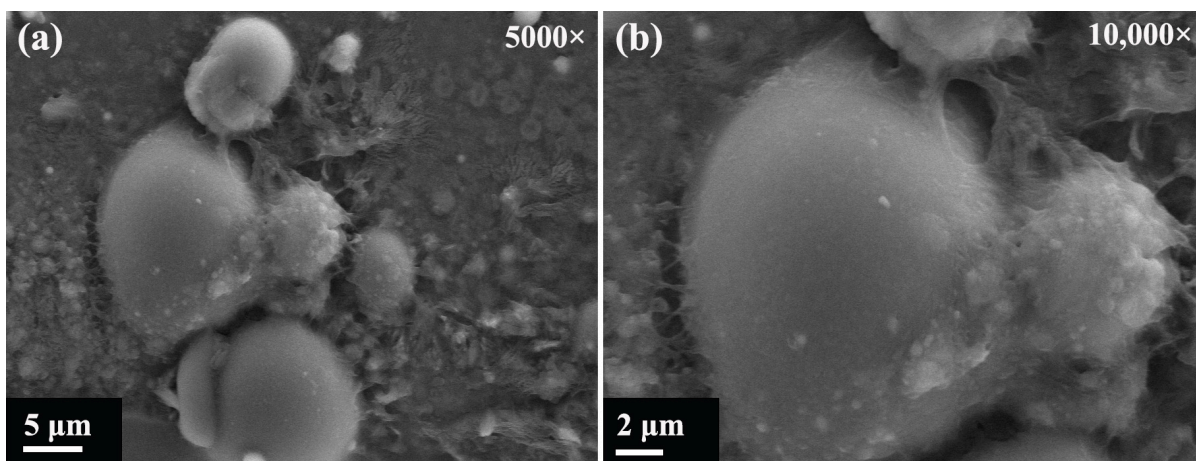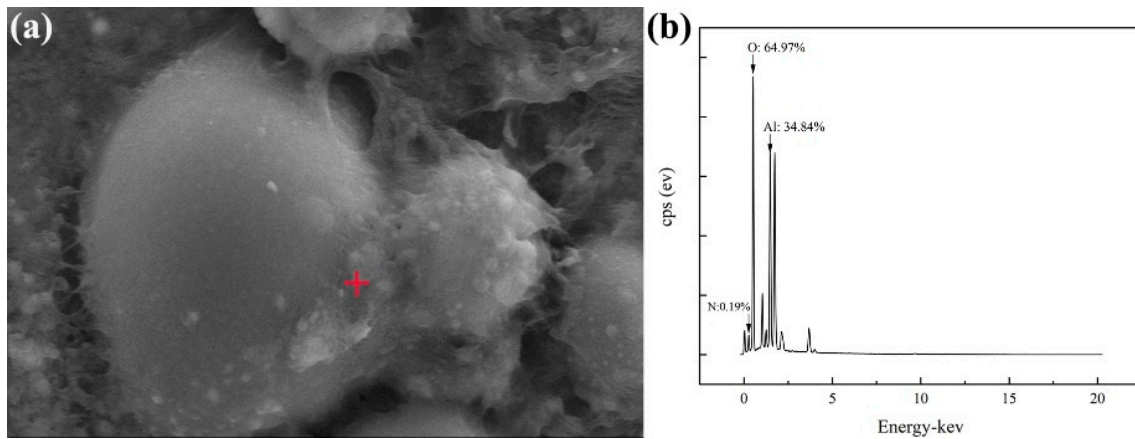**Figure 15.** Elemental mapping in the combustion residues of a single Al-Li alloy microparticle.

Figure 16. SEM photographs of daughter Al-Li alloy residues: (**a**) 5000×; (**b**) 10,000×.

Figure 17. EDS analysis of daughter Al-Li alloy residues. (**a**) SEM morphology; (**b**) EDS spectrum.

3.3. Discussion of Ignition and Combustion Mechanism

3.3.1. Ignition Mechanism

In this work, it was experimentally revealed that the ignition temperature of Al-Li alloy is lower than that of Al (Figure 6) and the increase in pressure shortens the ignition delay. Theoretically, for the ignition of a laser-induced individual microparticle, from the perspective of energy balance, the temperature rise can be expressed as:

$$cm\frac{dT}{dt} = \dot{Q}_L + \dot{Q}_{HSR} + \dot{Q}_{melt} + \dot{Q}_{vap} + \dot{Q}_{loss} \tag{3}$$

where c, m, and T are the heat capacity, mass, and temperature of the microparticle, respectively, and t is the time. $\dot{Q}_L$, $\dot{Q}_{HSR}$, $\dot{Q}_{melt}$, $\dot{Q}_{vap}$, and $\dot{Q}_{loss}$ represent the effective laser radiation power acting on the microparticle, the heat generated by the heterogeneous surface reaction (HSR), the melting heat, the latent heat of vaporization, and the heat loss to the cool air, respectively.

As the operation conditions remained the same, the heat generated by the HSR plays a crucial role in igniting the microparticle, which can be written as [43]:

$$\dot{Q}_{HSR} = A_1 e^{(-E_a/RT)} \tag{4}$$

where A_1 is the pre-exponential coefficient, E_a is the activation energy, and R is the universal gas constant, 8.314 J/(mol·K). On the basis of the TG data (Figure 6), the initial oxidation temperature of the Al-Li alloy is lower than that of Al, which means the activation energy of the alloy with Li added in air is less than that of pure Al, suggesting that the addition of Li promotes the initial reaction and increases the heat generated by the HSR. Moreover, the ignition temperature of Al-Li is lower (Figure 6), which means that the time to reach the critical ignition temperature in Equation (2) shortens, that is, the ignition delay becomes shorter, as compared to Al.

As the ignition laser power (density) increases, the temperature of the microparticle rises at a high rate (obtained using Equation (3)). This leads to a high release rate of the HSR (obtained using Equation (4)), which heats the microparticle. Thus, the temperature increases more quickly until the ignition temperature. This results in a reduction in the ignition delay time. Similarly, as the operating pressure increases, the reaction rate of the microparticle in air accelerates, the time to reach the critical ignition temperature in Equation (3) advances, and the ignition delay shortens.

The Al-Li alloy predominantly undergoes gas-phase combustion at the moment of ignition. This is different from the ignition pattern of a single Al particle under the same experimental conditions, which is dominated by a heterogeneous surface reaction [36]. For micron-sized Al-Li binary alloy particles, under laser heating, the internal temperature of the microparticles quickly reaches the melting points of Li and Al and the boiling point of Li

in a sequence (the melting point and boiling point of Li are 453 K and 1643 K, respectively; the melting point and boiling point of Al are 933 K and 2680 K, respectively) [44]. As the Li vaporizes and the gaseous Li diffuses towards the air, gas-phase ignition occurs. Therefore, the addition of Li benefits the ignition of Al-Li alloy microparticles, even at low contents of Li (1.0 wt.%).

3.3.2. Combustion Mechanism

The combustion of a single micron-sized Al-Li alloy particle in air can be divided into four stages (Figures 8 and 12) at both low pressure and high pressure: melting, gasification, diffusion combustion, and extinction. During combustion, Al-Li alloy microparticles undergo the microexplosion phenomenon similar to multicomponent hydrocarbon liquid fuels [45]. According to the experimental results stated above, a schematic diagram of the combustion route of an individual micron-sized Al-Li alloy particle in air is proposed, as shown in Figure 18.
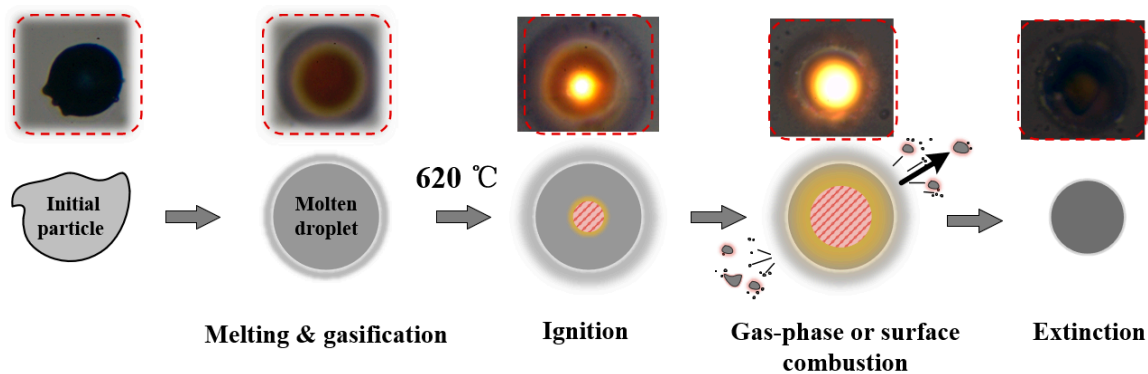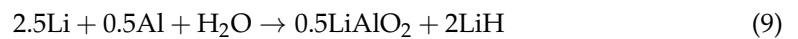

Figure 18. Schematic diagram of combustion route of single Al-Li alloy microparticles in air.

For a micron-sized Al particle, due to its high volumetric heat capacity, it usually needs to reach or approximate the melting point (~2350 K) of the Al_2O_3 shell to achieve ignition [4,30], and its combustion usually occurs on the surface, without an obvious microexplosion. However, for an Al-Li alloy microparticle, during melting, the Li in the Al-Li droplet gradually vaporizes and forms bubbles inside the microparticle owing to the limitation of the oxide layer (shell). When the expansion pressure inside the bubble quickly increases and exceeds the surface tension of the molten Al droplet, the breakup of the surface occurs. Thus, the molten Al is constantly sprayed from the core. If the pressure is much higher than the surface tension, unloading leads to the occurrence of a microexplosion [22]. After the microexplosion, the remaining Al-Li alloy experiences repetitive processes until extinction. Moreover, during the melting of Al-Li alloy microparticles, on the surface oxide layer, cracks appear earlier, which give way to the diffusion of oxygen atoms (inward), and Al and Li cations (outward), resulting in ignition. It is worth noting that Li cations have a higher diffusion rate than Al cations; thus, they can diffuse to the damaged oxide layer earlier and oxidize with the surrounding oxidants.

The ambient atmosphere plays a vital role in the combustion of Al-Li alloy microparticles. In air, aside from O_2, the N_2, CO_2, and gaseous H_2O also react with Li. The reaction equations of Li in air are listed as follows [37]:

$$4Li + O_2 \rightarrow 2Li_2O \tag{5}$$

$$6Li + N_2 \rightarrow 2Li_3N \tag{6}$$

$$Li_2O + CO_2 \rightarrow Li_2CO_3 \tag{7}$$

$$2Li + H_2O \rightarrow Li_2O + H_2 \tag{8}$$

$$2.5Li + 0.5Al + H_2O \rightarrow 0.5LiAlO_2 + 2LiH \tag{9}$$

To simplify the analysis, other than reaction Equation (5), herein, the reaction Equation (6) was also considered. To assess the influence of N_2 on the combustion reaction of Al-Li, an experiment was conducted in a N_2 atmosphere. Figure 19 shows the representative snapshots of the combustion process of a single Al-Li alloy microparticle in a N_2 atmosphere. Similar video on the combustion of a single Al-Li alloy microparticle can be found in Supplementary Material Video S2. It was observed that there was a large bright ignition point above the microparticle surface at 1214.2 ms (Figure 19d). The gaseous flame gradually propagated, covered the microparticle, and remained stable. The coverage of combustion products was more than 4–5 times greater than the initial particle size. During combustion, a reduction in the intensity and number of microexplosions was observed when Al-Li alloy microparticles burned in N_2, unlike the extreme intensity and high frequency in air. A similar difference in the intensity and frequency of microexplosions for Al-Zr alloy microparticles in air and in N_2 was also reported by Wainwright et al. [22]. They found that, in air, the Al-Zr alloy microparticles synthesized by mechanical milling and physical vapor deposition (PVD) exhibited primary, secondary, and tertiary microexplosions. While in Ar + O_2, Ar + N_2, and Ar environments, the microexplosion exhibited a weak intensity and low frequency. This reduction correlates well with the N_2 dependencies for the added metal elements in the alloy. In this experiment, Al scarcely reacted with N_2 to form the corresponding nitride (AlN) [46], while Li was chemically active and reacted with N_2 to form the nitride at relatively low temperatures [25]. In air, the reaction of Li and O_2 in reaction Equation (5) was stronger than the reaction of Li and N_2 in reaction Equation (6). Therefore, during melting, a part of N_2 in air dissolves in the molten droplet, resulting in a violent microexplosion. However, in pure N_2, the reaction of Li and N_2 decreases the solubility of N_2 in the molten droplet, minimizing bubble growth and the probability of a microexplosion. The probability of microexplosive behavior in N_2 is much lower than in air. Detailed statistics are not available in the current work but will be investigated in the future.
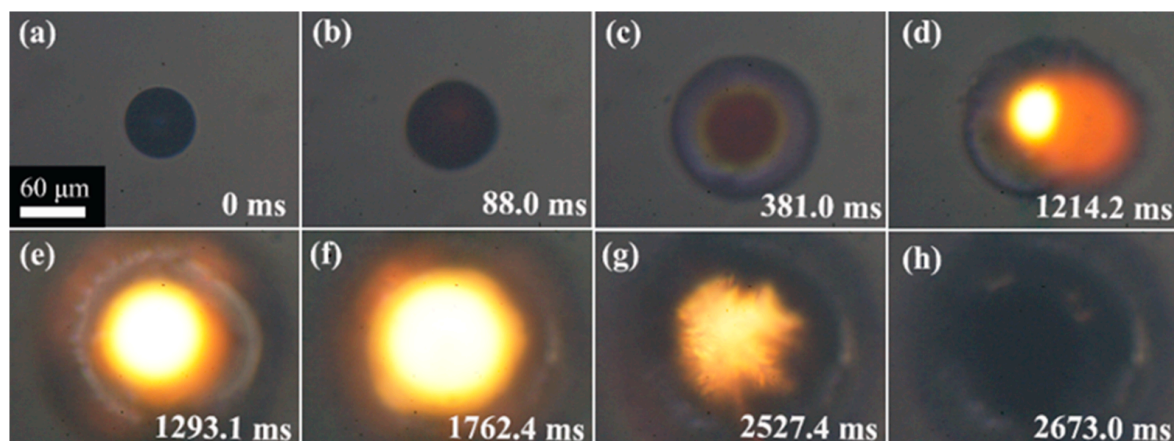
Figure 19. (**a**–**h**) Representative snapshots of a single Al-Li alloy microparticle burned in N_2.

The characteristic parameters of single Al-Li alloy microparticles burned in air and in N_2 were compared in 10 runs of repetitive experiments under a laser power of 2000 mW. The results are listed in Table 2. The ignition delay time of Al-Li alloy microparticles in N_2 increased, the gas-phase combustion time reduced, and the total combustion time increased. Compared with air, the ignition probability of Al-Li alloy in N_2 was ~30%, with a reduction of 68.4%. Since the content of Li in Al-Li alloy is less (~1%) and Al does not easily react

with the N_2 under the same conditions, N_2 hinders the combustion of the Al-Li alloy in the subsequent stage.

Table 2. Ignition and combustion characteristics of single Al-Li alloy microparticles in air and in N_2.

Atmosphere	Ignition Probability	Averaged Ignition Delay Time (s)	Burn Time (s)
Air	95%	0.483	2.223
N_2	30%	1.350	2.380

The pressure affects the combustion behavior of the microparticles and the adiabatic flame temperature [47,48]. The elevation of the pressure can significantly increase the probability of a microexplosion in microparticles (Figure 11). According to the diffusion reaction mechanism, with the increase in ambient pressure, the diffusion rate of external oxygen atoms to the inside of the particles increases, and the migration rates of Al and Li cations to the outside also increases, so the oxidation reaction rate of Al-Li alloy is accelerated. Moreover, in the pressurized environment, the average free path between gas molecules is shortened, the probability of microexplosion of Al-Li alloy microparticles is significantly increased, and the reaction rate becomes faster. Some microparticles demonstrate vigorous microexplosion behavior even before they fully burn, thus significantly reducing agglomeration and improving the combustion efficiency.

4. Conclusions

In this paper, the typical combustion processes of single micron-sized Al-Li binary alloy particles in air were observed at high temporal and spatial resolutions using self-built experimental apparatus, and the effects of atmosphere (air and N_2) and pressure on the ignition and combustion characteristics of Al-Li alloy were studied. Through analysis and discussion, the following conclusions can be made:

(1) The ignition temperature of the Al-Li alloy is lower than that of Al. The increase in laser power (density) can significantly improve the ignition probability. The combustion behavior is mainly characterized as a mixed mode, including heterogeneous surface combustion and homogeneous gas-phase combustion in air. The addition of Li promotes the occurrence of gas-phase combustion (AlO emission lines) with a microexplosion, promotes Al burn-out, and increases combustion efficiency. Al-Li alloys burned in N_2 exhibit a lower probability of ignition, a lower radiation intensity, and a reduced microexplosive behavior than in air;

(2) The ignition and combustion of Al-Li alloy microparticles can be promoted by increasing the air pressure. The higher the pressure, the shorter the ignition delay time and burn time of microparticles, which follows an exponential decay relationship. The increase in pressure results in a higher radiation intensity of the combustion flame and more chance of a microexplosion. The combustion temperatures of microparticles at high pressure are lower than those at atmospheric pressure owing to the microexplosion. The elevated pressure stabilized the microexplosion intensity, the combustion temperature, and the burn time in cool air.

Author Contributions: Conceptualization, X.H. and S.L.; methodology, X.H. and S.L.; investigation, D.X., F.W., S.L., X.H., H.L. and Y.G.; data curation, D.X., F.W. and S.L.; writing—original draft preparation, D.X., S.L. and X.H.; writing—review and editing, S.L. and X.H.; visualization, D.X.; supervision, S.L., X.H., F.W. and Y.G.; funding acquisition, S.L., X.H., F.W. and H.L. All authors have read and agreed to the published version of the manuscript.

References

1. Yetter, R.A.; Risha, G.A.; Son, S.F. Metal particle combustion and nanotechnology. *Proc. Combust. Inst.* **2009**, *32*, 1819–1838. [CrossRef]
2. Dreizin, E. Phase changes in metal combustion. *Prog. Energy Combust. Sci.* **2000**, *26*, 57–78. [CrossRef]
3. Rozenband, V.I.; Vaganova, N.I. A strength model of heterogeneous ignition of metal particles. *Combust. Explos. Shock. Waves* **1992**, *28*, 113–118. [CrossRef]
4. Fedorov, A.V.; Kharlamova, Y.V. Ignition of an Aluminum Particle. *Combust. Explos. Shock. Waves* **2003**, *39*, 544–547. [CrossRef]
5. Hickman, S.; Brewster, M. Oscillatory combustion of aluminized composite propellants. *Symp. (Int.) Combust.* **1996**, *26*, 2007–2015. [CrossRef]
6. Dong, H.; Zhumei, S. Study of the Fast Reaction Characteristics of Aluminized PETN Explosive Powders. *Combust. Flame* **1996**, *105*, 428–430. [CrossRef]
7. Yagodnikov, D.A.; Voronetskii, A.V.; Sarab'ev, V.I. Ignition and combustion of pyrotechnic compositions based on micro- and nanoparticles of aluminum diboride in airflow in a two-zone combustion chamber. *Combust. Explos. Shock. Waves* **2016**, *52*, 300–306. [CrossRef]
8. Sippel, T.R.; Son, S.F.; Groven, L.J. Altering Reactivity of Aluminum with Selective Inclusion of Polytetrafluoroethylene through Mechanical Activation. *Propellants, Explos. Pyrotech.* **2012**, *38*, 286–295. [CrossRef]
9. Rubio, M.A.; Gunduz, I.E.; Groven, L.J.; Sippel, T.R.; Han, C.W.; Unocic, R.R.; Ortalan, V.; Son, S.F. Microexplosions and ignition dynamics in engineered aluminum/polymer fuel particles. *Combust. Flame* **2017**, *176*, 162–171. [CrossRef]
10. Dreizin, E.L. Metal-based reactive nanomaterials. *Prog. Energy Combust. Sci.* **2009**, *35*, 141–167. [CrossRef]
11. Sundaram, D.S.; Yang, V.; Zarko, V.E. Combustion of nano aluminum particles (Review). *Combust. Explos. Shock. Waves* **2015**, *51*, 173–196. [CrossRef]
12. Babuk, V.; Dolotkazin, I.; Gamsov, A.; Glebov, A.; DeLuca, L.T.; Galfetti, L. Nanoaluminum as a Solid Propellant Fuel. *J. Propuls. Power* **2009**, *25*, 482–489. [CrossRef]
13. Sippel, T.R.; Son, S.F.; Groven, L.J. Aluminum agglomeration reduction in a composite propellant using tailored Al/PTFE particles. *Combust. Flame* **2014**, *161*, 311–321. [CrossRef]
14. Ao, W.; Liu, P.; Liu, H.; Wu, S.; Tao, B.; Huang, X.; Li, L.K.B. Tuning the agglomeration and combustion characteristics of alu-minized propellants via a new functionalized fluoropolymer. *Chem. Eng. J.* **2020**, *382*, 122987. [CrossRef]
15. Foley, T.J.; Johnson, C.E.; Higa, K.T. Inhibition of Oxide Formation on Aluminum Nanoparticles by Transition Metal Coating. *Chem. Mater.* **2005**, *17*, 4086–4091. [CrossRef]
16. Tian, B.; Zhang, J.; Bi, J.; Gu, N.; Xu, T. Fabrication of Fe–Al composite powder by electroless iron plating. *J. Synth. Crystallogr.* **2008**, *4*, 825.
17. Zhang, D.; Zou, H.; Cai, S. Effect of Iron Coating on Thermal Properties of Aluminum-Lithium Alloy Powder. *Propellants Explos. Pyrotech.* **2017**, *42*, 953–959. [CrossRef]
18. Sippel, T.R.; Son, S.F.; Groven, L.J.; Zhang, S.; Dreizin, E. Exploring mechanisms for agglomerate reduction in composite solid propellants with polyethylene inclusion modified aluminum. *Combust. Flame* **2015**, *162*, 846–854. [CrossRef]
19. Ao, W.; Fan, Z.; Liu, L.; An, Y.; Ren, J.; Zhao, M.; Liu, P.; Li, L.K. Agglomeration and combustion characteristics of solid composite propellants containing aluminum-based alloys. *Combust. Flame* **2020**, *220*, 288–297. [CrossRef]
20. Shoshin, Y.L.; Dreizin, E.L. Particle combustion rates for mechanically alloyed Al–Ti and aluminum powders burning in air. *Combust. Flame* **2006**, *145*, 714–722. [CrossRef]
21. Shoshin, Y.L.; Trunov, M.A.; Zhu, X.; Schoenitz, M.; Dreizin, E.L. Ignition of aluminum-rich Al–Ti mechanical alloys in air. *Combust. Flame* **2006**, *144*, 688–697. [CrossRef]
22. Wainwright, E.R.; Schmauss, T.A.; Lakshman, S.V.; Overdeep, K.R.; Weihs, T.P. Observations during Al:Zr composite particle combustion in varied gas environments. *Combust. Flame* **2018**, *196*, 487–499. [CrossRef]
23. Huang, X.; Yang, Y.; Hou, F.; Li, S.; Qin, Z.; Zhao, F. Laser-Induced Ignition and Combustion of Al−Mg Alloy Powder Prepared by Melt Atomization. *Propellants Explos. Pyrotech.* **2020**, *45*, 1645–1653. [CrossRef]
24. Moore, J.T.; Turns, S.R.; Yetter, R.A. Combustion of lithium–aluminum alloys. *Combust. Sci. Technol.* **2005**, *177*, 627–669. [CrossRef]
25. Zhu, Y.; Le, W.; Zhao, W.; Ma, X.; Liu, D.; Li, J.; Jiao, Q. Promising fuels for energetics: Spherical Al-Li powders with high reactivity via incorporation of Li. *Fuel* **2022**, *323*, 124393. [CrossRef]
26. Diez, G.A.; Manship, T.D.; Terry, B.C.; Gunduz, I.E.; Son, S.F. Characterization of an Aluminum–Lithium-Alloy-Based Composite Propellant at Elevated Pressures. *J. Propuls. Power* **2021**, *37*, 332–337. [CrossRef]

27. Blackman, A.W.; Kuehl, D.K. Use of Binary Light Metal Mixtures and Alloys as Additives for Solid Propellants. *ARS J.* **1961**, *31*, 1265–1272. [CrossRef]
28. Terry, B.C.; Sippel, T.R.; Pfeil, M.A.; Gunduz, I.E.; Son, S.F. Removing hydrochloric acid exhaust products from high per-formance solid rocket propellant using aluminum-lithium alloy. *J. Hazard. Mater.* **2016**, *317*, 259–266. [CrossRef]
29. Terry, B.; Gunduz, I.; Pfeil, M.; Sippel, T.; Son, S. A mechanism for shattering microexplosions and dispersive boiling phenomena in aluminum–lithium alloy based solid propellant. *Proc. Combust. Inst.* **2017**, *36*, 2309–2316. [CrossRef]
30. Li, S.; Huang, X.; Zhou, D. Experiments and Numerical Calculations on Laser-Induced Ignition of Single Micron-Sized Alu-Minum Fuel Particle. *Propellants Explos. Pyrotech.* **2017**, *42*, 523–531. [CrossRef]
31. Chen, J.-H.; Li, C.-R. *Thermal Analysis and Its Applications*; Science Press: Beijing, China, 1985.
32. Rufino, B.; Boulc'H, F.; Coulet, M.-V.; Lacroix, G.; Denoyel, R. Influence of particles size on thermal properties of aluminium powder. *Acta Mater.* **2007**, *55*, 2815–2827. [CrossRef]
33. Pranda, P.; Prandov, K.; Hlavacek, V. Combustion of fly-ash carbon: Part I. TG/DTA study of ignition temperature. *Fuel Process. Technol.* **1999**, *61*, 211–221. [CrossRef]
34. Hou, F.; Li, S.; Wang, Y.; Huang, X. Laser-Induced Ignition and Combustion of Individual Aluminum Particles Below 10 μm by Microscopic High-Speed Cinematography. *Processes* **2020**, *8*, 280. [CrossRef]
35. Li, S.; Pan, X.; Jiang, Y.; Chang, S.; Jin, X.; Yang, Y.; Huang, X.; Guo, Y. Ignition and Combustion Behaviors of High Energetic Polyhedral Boron Cluster. *Propellants Explos. Pyrotech.* **2019**, *44*, 1319–1326. [CrossRef]
36. Ahmad, M. Thermal oxidation behavior of an Al-Li-Cu-Mg-Zr alloy. *Met. Mater. Trans. A* **1987**, *18*, 681–689. [CrossRef]
37. Partridge, P.G. Oxidation of aluminium-lithium alloys in the solid and liquid states. *Int. Mater. Rev.* **1990**, *35*, 37–58. [CrossRef]
38. Li, S.; Zhuo, Z.; He, L.; Huang, X. Atomization characteristics of nano-Al/ethanol nanofluid fuel in electrostatic field. *Fuel* **2018**, *236*, 811–819. [CrossRef]
39. Schlöffel, G.; Eichhorn, A.; Albers, H.; Mundt, C.; Seiler, F.; Zhang, F. The effect of a shock wave on the ignition behavior of aluminum particles in a shock tube. *Combust. Flame* **2010**, *157*, 446–454. [CrossRef]
40. Beckstead, M.W. Correlating Aluminum Burning Times. *Combust. Explos. Shock. Waves* **2005**, *41*, 533–546. [CrossRef]
41. Braconnier, A.; Gallier, S.; Halter, F.; Chauveau, C. Aluminum combustion in CO_2-CO-N_2 mixtures. *Proc. Combust. Inst.* **2020**, *38*, 4355–4363. [CrossRef]
42. Kuryavtsev, V.M.; Sukhov, A.V.; Voronetskii, A.V.; Shpara, A.P. High-pressure combustion of metals (Three-zone model). *Combust. Explos. Shock. Waves* **1979**, *15*, 731–737. [CrossRef]
43. Huang, X.; Zhang, M.; Lin, C.; Yang, Y.; Li, S.; Li, H.; Yang, Y.; Qin, Z.; Zhao, F. Comparison on ignition and combustion of AlMgB composite fuel and B fuel. *Chem. Eng. J.* **2022**, *450*, 138133. [CrossRef]
44. Brzustowski, T.A.; Glassman, I. Spectroscopic Investigation of Metal Combustion. *Prog. Astronaut. Rocket.* **1964**, *15*, 41–73.
45. Lasheras, J.; Fernandez-Pello, A.; Dryer, F. Experimental observations on the disruptive combustion of free droplets of mul-ticomponent fuels. *Combus. Sci. Technol.* **1980**, *22*, 195–209. [CrossRef]
46. Desjardin, P.E.; Felske, J.D.; Carrara, M.D. Mechanistic Model for Aluminum Particle Ignition and Combustion in Air. *J. Propuls. Power* **2005**, *21*, 478–485. [CrossRef]
47. Bazyn, T.; Krier, H.; Glumac, N. Combustion of nanoaluminum at elevated pressure and temperature behind reflected shock waves. *Combust. Flame* **2006**, *145*, 703–713. [CrossRef]
48. Meda, L.; Marra, G.; Galfetti, L.; Severini, F.; De Luca, L. Nano-aluminum as energetic material for rocket propellants. *Mater. Sci. Eng.* **2007**, *27*, 1393–1396. [CrossRef]